Current bounds on baryogenesis from complex Yukawa couplings of light fermions

Shahaf Aharony Shapira*

Department of Particle Physics and Astrophysics, Weizmann Institute of Science, Rehovot 7610001, Israel

(Received 13 June 2021; accepted 22 March 2022; published 25 May 2022)

We calculate the contribution to the baryon asymmetry of the Universe (BAU) from a *CP*-violating source of the light quarks (charm, strange, down, up) and the electron, resulting from a dimension-six effective field theory term. We derive relevant bounds from the electric dipole moments of the electron and neutron to estimate the maximal contribution from each single-flavor modification. Current bounds show that the charm quark can generate at most $\mathcal{O}(1\%)$ of the BAU, while the lighter quarks and the electron contribute at much lower levels.

DOI: 10.1103/PhysRevD.105.095037

I. INTRODUCTION

The baryon asymmetry of the Universe (BAU) is defined and measured [1,2] to be

$$Y_B \equiv \frac{n_B - n_{\bar{B}}}{s} \approx (8.6 \pm 0.1) \times 10^{-11} \equiv Y_B^{\text{obs}}, \qquad (1)$$

where $n_{(\bar{B})B}$ is the (anti)baryon number density and s is the entropy density of the Universe. A nonvanishing value can be either the result of initial conditions, or dynamically generated during the early Universe. The former requires fine tuning and is inconsistent with inflation. The latter, which is the more acceptable mechanism to address the asymmetry, is called baryogenesis (See [3,4], for reviews).

There are three necessary conditions, known as the Sakharov conditions [5], that are required from any theory in order to explain such an imbalance: Baryon number violation, *C*-symmetry and *CP*-symmetry violation, and interactions out of thermodynamic equilibrium. Although the Standard Model (SM) meets all three criteria, the rate at which it contributes is far too small to account for the observed baryon asymmetry [6,7] due to two factors; the smooth crossover of the electroweak phase transition and the suppression from the Kobayashi-Maskawa mechanism of *CP* violation. Thus, if the baryon asymmetry was generated via electroweak baryogenesis, the electroweak phase transition had to be strongly first order and a new source of *CP* violation must exist at, or at least not far above, the electroweak scale.

New physics (NP) beyond the SM is highly motivated by several open questions in physics (e.g., dark matter, neutrino masses). However, despite the efforts made to discover new particles, none were found up to the TeV scale [8,9]. It is then plausible that NP is above the electroweak scale, and thus could be integrated out. This allows us to use Standard Model effective field theory (SMEFT) tools to explore higher-order terms, without being model dependent.

We add a *CP*-violating (CPV) phase using a dimension-six (dim-6) coupling of three Higgs fields to the SM charged fermions. The BAU is then proportional to the CPV source, which could be constrained by the electric dipole moment (EDM) of both the electron and neutron and by the Higgs boson decay and production rates. This was previously done for the third generation particles [10–12] and the muon [13]. Of that list, it was shown that the τ is the only sole contributor that can provide the entire observed value of the BAU [11,12]. We applied this procedure to evaluate the contribution from all of the SM particles, including the light quarks (charm, strange, down, up), and the electron, and discuss the results here.

This paper is organized as follows. First, we describe the SMEFT framework, including the complex dim-6 term and the CPV source it generates. We then outline key points in the process of electroweak baryogenesis, which are formulated by the two-step approach via the transport equations followed by the sphaleron process. Next, we present our numerical results for the contribution of a single flavor to the BAU. The contribution is later bounded using the experimental measurements of the electron and neutron EDMs and of various Higgs boson processes. Finally, we discuss our results and conclusions.

*shahaf.aharony@weizmann.ac.il

II. SMEFT FRAMEWORK

We examine the implications of adding the following effective dim-6 terms to the SM,

$$\mathcal{L}_{\text{eff Yuk}} = -\left(y_f + \frac{|H|^2}{\Lambda^2}(X_f^R + iX_f^I)\right)\overline{\psi_{Lf}}\psi_{Rf}H + \text{H.c.}, \quad (2)$$

where y_f is the dimension-4 (dim-4) Yukawa coupling, H is the SM Higgs field $H \sim (1,2)_{+1/2}$, Λ is the NP scale, X is the dim-6 Wilson coefficient and ψ is a SM fermion. In our notation, the lower index, f, denotes the flavor whereas the upper index distinguishes between the real (R) and imaginary (I) coefficients. We find it useful to define [12,13]

$$T_f^{R,I} \equiv \frac{v^2}{2\Lambda^2}\frac{X_f^{R,I}}{y_f}, \quad (3)$$

where $v = 246$ GeV is the vacuum expectation value (VEV) of the Higgs background field (h) defined $H = \frac{1}{\sqrt{2}}(0, v+h)^T$. Accordingly, the mass (m) and effective Yukawa coupling (λ) of each flavor can be defined and explicitly written as

$$\mathcal{L}_{\text{eff Yuk}} \supset -m_f\bar{\psi}_{Lf}\psi_{Rf} - \lambda_f\bar{\psi}_{Lf}\psi_{Rf}h + \text{H.c.}, \quad (4)$$

$$m_f = \frac{vy_f}{\sqrt{2}}(1 + T_f^R + iT_f^I), \quad \lambda_f = \frac{y_f}{\sqrt{2}}(1 + 3T_f^R + i3T_f^I). \quad (5)$$

In the mass basis, where $m_f \in \mathbb{R}$, they are given by [12,13]

$$m_f' = \frac{vy_f}{\sqrt{2}}\sqrt{(1+T_f^R)^2 + T_f^{I\,2}}, \quad (6)$$

$$\lambda_f' = \frac{y_f}{\sqrt{2}}\frac{(T_f^R+1)(3T_f^R+1) + T_f^I(3T_f^I+2i)}{\sqrt{(1+T_f^R)^2 + T_f^{I\,2}}}. \quad (7)$$

Throughout this work we will use the complex parameter κ_f, representing the deviation from the SM in the mass basis,

$$\kappa_f \equiv \frac{\lambda_f' v}{m_f'} = 3 - \frac{2}{1 + T_f^R + iT_f^I},$$
$$\kappa_f^I \equiv \text{Im}(\kappa_f) = \frac{2T_f^I}{(1+T_f^R)^2 + T_f^{I\,2}}. \quad (8)$$

Equivalently, one could express $\kappa_f = \frac{\lambda_f'}{\lambda_f'^{\text{SM}}}$ where, as in the SM, $\lambda_f'^{\text{SM}} \equiv \frac{m_f'}{v}$. It is convenient to use κ_f since the baryon asymmetry is proportional to the CPV source [S_f, Eq. (A8)] and therefore linear in κ_f^I [12],

$$Y_B \propto S_f \propto \text{Im}(m_f^* m_f') \propto \kappa_f^I. \quad (9)$$

In the above, we use the VEV insertion approximation [14], to leading order.

III. ELECTROWEAK BARYOGENESIS

By adding a complex effective Yukawa coupling to one of the fermions of the SM we introduce a CPV source to the model. The source depends on the background Higgs boson field h, which acquires a VEV. Here we assume that the electroweak phase transition is strongly first order, and describe h by the kink solution [Eq. (A10)]. This choice results with a CPV source that peaks mostly inside the nonvanishing VEV bubble. A schematic plot is given in Fig. 1. Namely, the CPV source generates a chiral asymmetry, mainly inside the broken phase. That asymmetry can be transformed into an abundance of baryons via the weak sphaleron, which is a nonperturbative effect of the SM. The rate of the weak sphaleron process is given by $\Gamma_{\text{ws}} \sim e^{-\langle h\rangle/T}T$ [15], where T is the temperature. Although the rate is exponentially suppressed inside the bubble, it is fast outside the bubble, during the early Universe. Therefore, for baryogenesis to occur at the electroweak phase transition, the chiral asymmetry should have propagated outside the bubble and into the symmetric phase [16]. Finally, as the bubble continues to expand, it eventually captures the resulting baryon asymmetry.

IV. TWO-STEP APPROACH

The dim-6 term described in Eq. (2) will affect the dynamics of the number densities, which are defined as the difference between the number densities of particles and antiparticles. This effect is the first step of the approach and is described via a set of transport equations. We generalize

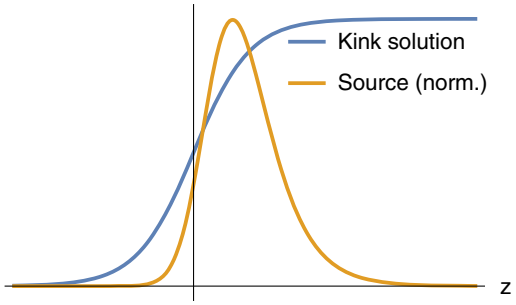

FIG. 1. Schematic description of the kink solution and its resulting CPV source along the distance from the bubble wall ($z = 0$). Blue: the kink solution for the background Higgs boson field, as given in Eq. (A10), orange: the resulting source, normalized.

the set given in [11] to include all the fermions of the SM in addition to the Higgs boson,

$$\begin{aligned}
\partial_\mu U_i^\mu \equiv \partial U_i &= -\Gamma_M^{U_i}\mu_M^{U_i} - \Gamma_Y^{U_i}\mu_Y^{U_i} + \Gamma_{ss}\mu_{ss} + S_{U_i},\\
\partial D_i &= -\Gamma_M^{D_i}\mu_M^{D_i} - \Gamma_Y^{D_i}\mu_Y^{D_i} + \Gamma_{ss}\mu_{ss} + S_{D_i},\\
\partial Q_i &= -\partial U_i - \partial D_i,\\
\partial E_i &= -\Gamma_M^{E_i}\mu_M^{E_i} - \Gamma_Y^{E_i}\mu_Y^{E_i} + S_{E_i},\\
\partial L_i &= -\partial E_i,\\
\partial h &= \sum_{i=1}^{3}\Gamma_Y^{U_i}\mu_Y^{U_i} - \sum_{i=1}^{3}\Gamma_Y^{D_i}\mu_Y^{D_i} - \sum_{i=1}^{3}\Gamma_Y^{E_i}\mu_Y^{E_i},
\end{aligned} \tag{10}$$

where U_R, D_R, and Q_L are the SM quark fields, E_R, and L_L are the SM charged lepton fields (the chirality is implicit hereafter), $\Gamma_{M,Y}$ are the relaxation and Yukawa rates, respectively, and S_f are the CPV sources. The chemical potentials are given by

$$\begin{aligned}
\mu_Y^{U_i} &= \frac{U_i}{k_{U_i}} - \frac{Q_i}{k_{Q_i}} - \frac{h}{k_h}, \qquad \mu_M^{U_i} = \frac{U_i}{k_{U_i}} - \frac{Q_i}{k_{Q_i}},\\
\mu_Y^{D_i} &= \frac{D_i}{k_{D_i}} - \frac{Q_i}{k_{Q_i}} + \frac{h}{k_h}, \qquad \mu_M^{D_i} = \frac{D_i}{k_{D_i}} - \frac{Q_i}{k_{Q_i}},\\
\mu_Y^{E_i} &= \frac{E_i}{k_{E_i}} - \frac{L_i}{k_{L_i}} + \frac{h}{k_h}, \qquad \mu_M^{E_i} = \frac{E_i}{k_{E_i}} - \frac{L_i}{k_{L_i}},\\
\mu_{ss} &= \sum_{i=1}^{3}\left(\frac{2Q_i}{k_{Q_i}} - \frac{U_i}{k_{U_i}} - \frac{D_i}{k_{D_i}}\right),
\end{aligned} \tag{11}$$

where k counts the finite temperature degrees of freedom. All of the benchmark parameters were taken from Ref. [17], and are presented in Appendix A. The solution of the transport equations is obtained by reduction of order [17], i.e., N second-order differential equations are written as a set of $2N$ first-order differential equations, and numerical diagonalization. By the second step of the approach the left-handed particles participate in the sphaleron process which generates a baryon asymmetry [Eq. (B14)]. The two-step procedure is summarized in more detail in Appendix B.

V. NUMERICAL RESULT

Our numerical calculation for the BAU yields

$$\begin{aligned}
Y_B(\kappa_f^I) = -Y_B^{\rm obs}\cdot(&-28\kappa_t^I + 11\kappa_\tau^I + 0.2\kappa_b^I + 0.1\kappa_\mu^I\\
&+0.03\kappa_c^I + 2\times10^{-4}\kappa_s^I + 3\times10^{-6}\kappa_e^I\\
&+4\times10^{-7}\kappa_d^I + 9\times10^{-8}\kappa_u^I).
\end{aligned} \tag{12}$$

This result agrees with previous analysis for the third-generation particles [12] and the muon [13], but also includes the rest of the charged SM fermions.

We point out that although quarks have (on average) larger dim-4 Yukawa couplings, which positively impact the CPV source, they also have more washout. It is the result of lower diffusion [18,19] and higher interaction rates, as well as an additional interaction via the strong sphaleron [20]. This important difference makes the charged leptons better candidates for producing the BAU, compared to quarks [11,12,21].

An interesting feature that holds only for the light fermions is that the ratio between contributions of different flavors of same type (either charged leptons or quarks) to the BAU is proportional to the ratio of the mass squared, up to 5%. For f_1, f_2 light flavors of same type, we get the following numerical result,

$$\frac{Y_B^{f_1}}{Y_B^{f_2}} \approx \left(\frac{m_{f_1}}{m_{f_2}}\right)^2 \frac{\kappa_{f_1}^I}{\kappa_{f_2}^I}. \tag{13}$$

The mass squared is explicitly introduced to the source term [See Eq. (A8)], which is otherwise almost identical for same type particles. However, it is nontrivial that the numerical solution of the transport equations is approximately linear with various fermionic sources, given they have different interaction rates. It is a consequence of the negligible difference between the light fermion rates (See Table III) and indeed, this relation does not hold for the third generation particles.

Moreover, the solution for every given κ_f^I is centered around a cancellation between the dim-6 and dim-4 contributions to m_f'. By rearranging the definition of κ_f^I [Eq. (8)], we get

$$(T_f^R + 1)^2 + \left(T_f^I - \frac{1}{\kappa_f^I}\right)^2 = \left(\frac{1}{\kappa_f^I}\right)^2. \tag{14}$$

(See inset of Fig. 2 for the geometrical interpretation.) The center of the circle, at $T_f^R = -1$, implies that the mass of the fermion is effectively generated by the imaginary part of the dim-6 term [See Eq. (6)]. This point requires a fine-tuned cancellation between the dim-4 Yukawa coupling and the real part of the dim-6 term. Furthermore, we do not expect this tension to be relaxed by introducing higher-order terms, as they have negligible contribution. Finally, the desired κ_f^I that saturates the contribution to the BAU to its observed value could correspond to an unfavorable solution, when demanding the theory to be perturbative. Let us denote the single flavor modification κ_f^I which satisfies $Y_B = Y_B^{\rm obs}$, according to Eq. (12), by κ_f^{I*}. The solution κ_f^{I*} corresponds to a circle in (T_f^R, T_f^I) space. By setting the mass m_f' [See Eq. (6)] to its measured value, we calculate the resulting dim-4 coupling y_f for each point on the circle, as a function of its central angle from the positive horizontal direction (θ). For some cases, depending on the particle and the position on the circle, it requires $y_f > 4\pi$ which in nonperturbative (See Fig. 2), rendering the analysis moot.

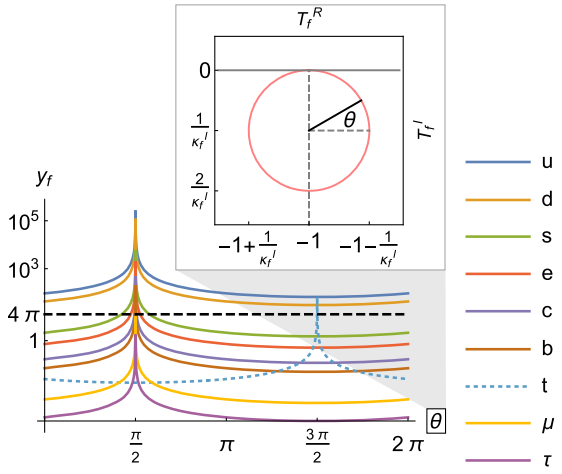

FIG. 2. *Main*: Dim-4 Yukawa coupling y_f as a function of θ (See inset). The coupling y_f is expressed by setting the mass m'_f to its measured value and κ_f^I to κ_f^{I*}. The region above the dashed black line $y_f = 4\pi$ is nonperturbative and is therefore considered unfavorable. The up and down quarks are nonperturbative throughout the entire range, which precludes them as a sole-source of the observed BAU. *Inset*: The geometrical interpretation of Eq. (14), for a given κ_f^I, is a circle in (T_f^R, T_f^I) space centered around $(-1, 1/\kappa_f^I)$ with radius $1/|\kappa_f^I|$. Each point on the circle is mapped to θ, its central angle from the positive horizontal direction. The plot corresponds to $\kappa_f^I < 0$ [See Eq. (12)].

A theoretical upper bound on $|\kappa_f^I|$ is produced by requiring there exists θ_p for which $y_f(\theta_p) \leq 4\pi$. Although this constraint is fairly weak, we present the perturbativity bound in Table I for comparison reasons. Note that $\theta = \frac{\pi}{2}$ ($\frac{3\pi}{2}$ for the top), which corresponds to $(-1, 0)$ in (T_f^R, T_f^I) space, is clearly unphysical and should be excluded. For large values of κ_f^{I*}, the radius of the circle, $1/|\kappa_f^{I*}|$, is too small to escape this critical region. We specifically point out the up and down quarks, for which there is no perturbative theory that can account for the observed BAU.

VI. BOUNDS

The implications of a nonzero κ_f^I are manifold; In addition to the generation of baryon asymmetry, which was discussed above, we focus on the contribution of a single κ_f^I to the EDMs of the electron and the neutron, and Higgs related measurements [31]. In this section we use these experimental results to constrain the maximal value of $|\kappa_f|$, assuming $\kappa_{\tilde{f}} = 1$ for all $\tilde{f} \neq f$. This will allow us to infer the maximal contribution, from a single flavor modification, to the BAU.

electron-Electric Dipole Moment (eEDM) Bound The upper bound (U.B.) obtained by the ACME Collaboration on the eEDM [28] is

$$|d_e^{\max}| = 1.1 \times 10^{-29}\ e\,\text{cm at 90\% C.L.}. \tag{15}$$

The contribution of the SM fermions, other than the top and the electron, to the eEDM is given by [30,32]

$$\frac{d_e}{e} \simeq 4N_c Q_f^2 \frac{\alpha}{(4\pi)^3} \frac{m_e m_f^2}{v^2 m_h^2} \left(\ln^2\left(\frac{m_f^2}{m_h^2}\right) + \frac{\pi^2}{3}\right)\kappa_f^I. \tag{16}$$

The contribution of the top quark to the eEDM is given by [33]

$$\frac{d_e}{e} \simeq 9.4 \times 10^{-27}\kappa_t^I\ \text{cm}. \tag{17}$$

The contribution of the electron to the eEDM is given by [34]

$$\frac{d_e}{e} \simeq 5.1 \times 10^{-27}\kappa_e^I\ \text{cm}. \tag{18}$$

TABLE I. The BAU calculated following the full set of transport equations. Y_B^f is the BAU resulting from a single source S_f. Collider constraints are at ~95% C.L. [12,22–27] (for details see Table II). EDM constraints are at 90% C.L. [28,29] for all, except for the bottom and charm, for which the nEDM constraints are at 68% C.L. [30]. Perturbativity bounds are calculated by setting m'_f to its measured value and demanding that there exists θ_p for which $y_f(\theta_p) = 4\pi$.

S_f, f	BAU, Y_B^f $\times\kappa_f^I$	Collider $\lvert\kappa_f\rvert^{\max}$	eEDM $\lvert\kappa_f^I\rvert^{\max}$	nEDM $\lvert\kappa_f^I\rvert^{\max}$	Perturbativity $\lvert\kappa_f^I\rvert^{\max}$	$Y_B^{f\,\max}$ $\times Y_B^{\text{obs}}$
τ	-9.9×10^{-10}	1.1	0.3	⋯	2×10^3	3.37
μ	-1.0×10^{-11}	1.3	31	⋯	4×10^4	0.16
b	-2.1×10^{-11}	1.7	0.2	7.4	1×10^3	5.8×10^{-2}
t	$+2.4 \times 10^{-9}$	1.1	1.2×10^{-3}	⋯	25	3.3×10^{-2}
c	-2.7×10^{-12}	3.9	0.4	15.5	3×10^3	1.1×10^{-2}
s	-1.6×10^{-14}	30	109	4.5	5×10^4	8×10^{-4}
d	-3.8×10^{-17}	621	2.3×10^4	0.14	9×10^5	6×10^{-8}
u	-8.2×10^{-18}	1326	2.2×10^4	0.6	2×10^6	6×10^{-8}
e	-2.5×10^{-16}	265	2.2×10^{-3}	⋯	9×10^6	6×10^{-9}

VII. NEUTRON-ELECTRIC DIPOLE MOMENT (NEDM) BOUND

The U.B. obtained by the nEDM collaboration on the nEDM [29] is

$$|d_n^{\max}| = 1.8 \times 10^{-26}\ e\,\mathrm{cm\ at\ 90\%\ C.L.}. \tag{19}$$

This bound constrains only the κ_f^I of the quarks. The implications of the nEDM bound on $\kappa_{u,d,s}^I$ were calculated in [35]. Here we show the 90% confidence level (C.L.) bound, updated to the latest measurement,

$$|\kappa_u^I| \lesssim 0.6, \qquad |\kappa_d^I| \lesssim 0.14, \qquad |\kappa_s^I| \lesssim 4.5. \tag{20}$$

We also update the 68% C.L. bounds on $\kappa_{b,c}^I$ given in [30], assuming $\kappa_{b,c}^R = 0$,

$$|\kappa_b^I| \lesssim 7.4, \qquad |\kappa_c^I| \lesssim 15.5. \tag{21}$$

We used the weakest constraint, given for negative sign of the Weinberg-operator, with the short-distance theory uncertainty (in quadrature) for the charm (bottom).

VIII. COLLIDER CONSTRAINTS

The signal strength $\mu_{h\to f\bar{f}}$ can be written in terms of the production rate σ and branching ratio $\mathcal{B}$ as

$$\mu_{i,h\to f\bar{f}} \equiv \frac{\sigma_i(pp\to h)\mathcal{B}(h\to f\bar{f})}{\sigma_i^{\mathrm{SM}}(pp\to h)\mathcal{B}^{\mathrm{SM}}(h\to f\bar{f})}. \tag{22}$$

We first use measurements of $\mu_{h\to\ell\bar{\ell}}$ to constraint $|\kappa_\ell|$ directly, for the charged leptons and bottom quark, denoted $\ell = \tau, \mu, e, b$. Since the contribution of light fermions to the production rate of the Higgs boson is insignificant already at dim-4, we can safely neglect their effect via the dim-6 term. Regarding the bottom quark, this approximation neglects its 1% loop contribution to gluon-gluon fusion (ggF) [22]. However, the eEDM bound, in this case, turns out to be more significant [12]. We therefore approximate

$$\mu_{h\to\ell\bar{\ell}} \approx \frac{\mathcal{B}(h\to\ell\bar{\ell})}{\mathcal{B}^{\mathrm{SM}}(h\to\ell\bar{\ell})}. \tag{23}$$

It is then straightforward to translate the U.B. of the signal strength to the maximal value of $|\kappa_\ell|$ using [34]

$$\mu_{h\to\ell\bar{\ell}} = \frac{|\kappa_\ell|^2}{1+(|\kappa_\ell|^2-1)\mathcal{B}(h\to\ell\bar{\ell})^{\mathrm{SM}}}. \tag{24}$$

The next class is that of the light quarks $q = u, c, d, s$, which could only be bounded via its effect on the total decay width of the Higgs boson. When NP interacts only with q, i.e., $\kappa_f = 1$ for all $f \neq q$, the signal strength of f is modified as

$$\mu_{h\to f\bar{f}} = \frac{1}{1+(|\kappa_q|^2-1)\mathcal{B}(h\to q\bar{q})^{\mathrm{SM}}}. \tag{25}$$

As the lower bound of the signal strength $\mu_{h\to f\bar{f}}$ tends to one, the upper bound on $|\kappa_q|$ gets stronger. Currently, the experimental lower bound closest to unity is that of the bottom, $\mu_{h\to b\bar{b}} = 1.04 \pm 0.20$ [23] (see Table II). Therefore, we use $\mu_{h\to b\bar{b}}$ to solve the above equation and constrain $|\kappa_q|$.

Lastly, the single flavor modification of the top quark is bounded using the dominant, top mediated, production modes of the Higgs boson; ggF and $t\bar{t}h$. The top affects both the production rate $(\sigma/\sigma^{\mathrm{SM}} = |\kappa_t|^2)$, as well as the total decay width of the Higgs boson [Eq. (25)]. The overall

TABLE II. Collider limits on the signal strength $\mu_{h\to f\bar{f}}$ from which we evaluate the U.B. at ~95% C.L.. Combined with the SM prediction for the branching ratio, $\mathcal{B}^{\mathrm{SM}}$, we constrain $|\kappa_f|$ using Eq. (24) for $\ell = \tau, \mu, e, b$, Eq. (25) for $q = u, c, d, s$, and Eq. (26) for the top. We extrapolated $\mathcal{B}^{\mathrm{SM}}$ for the electron (up and down quarks) from that of the muon (strange), using $\mathcal{B}_{h\to f\bar{f}}^{\mathrm{SM}} \propto m_f^2$.

Channel	Experiment	$\mu_{h\to f\bar{f}}^{\text{best fit}}$	$\mu_{h\to f\bar{f}}^{\text{U.B.}}$	$\mathcal{B}_{h\to f\bar{f}}^{\mathrm{SM}}$
$h\to\tau\bar{\tau}$	ATLAS + CMS	0.91 ± 0.13 [12]	1.1	6.3×10^{-2} [22]
$h\to\mu\bar{\mu}$	ATLAS CMS	1.2 ± 0.6 [24] 1.19 ± 0.44 [25]	1.8	2.2×10^{-4} [22]
$h\to b\bar{b}$	CMS	1.04 ± 0.20 [23]	1.4	0.58 [22]
$ggF + t\bar{t}h$	ATLAS + CMS	1.09 ± 0.08 [12]	1.2	$\mathcal{B}(h\to gg)^{\mathrm{SM}} = 8.2\times10^{-2}$ [22]
$h\to c\bar{c}$				2.9×10^{-2} [22]
$h\to s\bar{s}$		using $\mu_{h\to b\bar{b}} \geq 0.71$ [23]		4.40×10^{-4} [26]
$h\to d\bar{d}$				1.1×10^{-6} [26]
$h\to u\bar{u}$				2.4×10^{-7} [26]
$h\to e\bar{e}$	ATLAS	$\mathcal{B}^{\text{U.B.}} = 3.6\times10^{-4}$ [27]	7.0×10^{4}	5.1×10^{-9} [22]

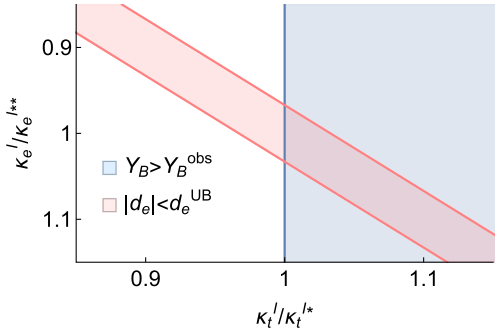

FIG. 3. The interplay between the electron and the top could allow the top to saturate the observed BAU via $\kappa_t = 1 + i\kappa_t^{I*}$, while canceling the contribution of κ_t^{I*} to the eEDM using $\kappa_e = 1 + i\kappa_e^{I**}$. Accordingly, κ_e^{I**} is set such that d_e, i.e., the sum of equations (17) and (18), equals zero. Since the next leading bound on both particles is orders of magnitude weaker, such cancellation would be difficult to detect.

effect can be written as [12]

$$\mu_{\mathrm{ggF}+t\bar{t}h} = \frac{|\kappa_t|^2}{1 + (|\kappa_t|^2 - 1)\mathcal{B}(h \to g\bar{g})^{\mathrm{SM}}}. \tag{26}$$

IX. RESULTS

We present our results in Table I. The first prominent result is that no light charged fermion could give the dominant contribution to the BAU. Of all the SM charged fermions only the τ could produce 100% of the observed BAU [11,12]. The next in importance can be the μ [13], which brings us to consider the relatively negligible effect of the light quarks. In addition to their low contribution to the BAU, the bounds on light quarks are comparable to these of the leptons, and thus their maximal percentage is relatively small.

That being said, one could consider two flavor modification, in which case the electron has a special feature. Assuming the numerical result is linear with multiple CPV sources of different species, the electron could cancel the contribution of some particles to the eEDM, while leaving the contribution to the BAU essentially unchanged. When combined, the interference allows particles that are constrained mostly by the eEDM, such as the top [12], to account for the BAU. For example, for $\kappa_t^{I*} \approx 0.04$, the top generates Y_B^{obs}, while $\kappa_e^{I**} \approx -0.06$ cancels the top's contribution to the eEDM (See Fig. 3). Because of possible cancellation, it is much harder to exclude such an elusive hypothetical scenario.

X. CONCLUSIONS

We consider the CPV source resulting from a dim-6 SMEFT term which couples three Higgs fields to the SM fermions. We apply the procedure described in Ref. [17] to evaluate the complete set of single flavor modifications from all of the SM charged fermions.

We deduce that although a larger dim-4 Yukawa coupling enhances the CPV source, quarks have more washout than leptons and are therefore less favorable candidates to produce the BAU. Moreover, to saturate Y_B^{obs}, some of the particles require nonperturbative dim-4 Yukawa couplings, e.g., the up and down quarks, and are therefore unequivocally ruled out as sole contributors via this mechanism.

Constrained by U.Bs of the electron and neutron EDMs and measurements of various Higgs boson processes, we evaluate the maximal contribution from each single flavor modification (See Table I). We conclude that the τ is the only candidate able to produce the observed BAU [11,12]. Other than the μ, which could provide up to 16% Y_B^{obs} [13], the rest of the charged fermions produce negligible contributions (less than 6% Y_B^{obs}).

An interplay of different flavors could relax current bounds to allow the observed baryon asymmetry be accounted for by a CPV Yukawa coupling. Specifically, the interplay of the top and the electron could allow the top to saturate Y_B^{obs}.

ACKNOWLEDGMENTS

We are grateful to Yossi Nir and Yehonatan Viernik for helpful discussions.

APPENDIX A: BENCHMARK PARAMETERS

The input used for this work is the following:

(a) Coupling constant at nucleation temperature [10]:

$$g_s = 1.23, \qquad g = 0.65, \qquad g' = 0.36. \tag{A1}$$

(b) Bubble wall velocity and width [11]:

$$v_w = 0.05, \qquad L_w = 0.11\ \mathrm{GeV}^{-1}. \tag{A2}$$

(c) VEV during nucleation [10] and at 0 temperature:

$$v_N = 152\ \mathrm{GeV}, \qquad v_0 = 246\ \mathrm{GeV}. \tag{A3}$$

(d) The SM fermion masses were taken from [1].

(e) The diffusion coefficients of leptons (ℓ) and quarks (q) are [16]:

$$D_{\ell_L} = D_h = \frac{100}{T}, \qquad D_{\ell_R} = \frac{380}{T}, \qquad D_{q_L} = D_{q_R} = \frac{6}{T}. \tag{A4}$$

(f) The Mass and Yukawa rates are given in Table III. These interaction rates are calculated for $T_I = T_R = 0$.

(g) The weak sphaleron rate [36]

$$\Gamma_{\rm ws} = 6\underbrace{\kappa}_{\sim 20}\underbrace{\alpha_w^5}_{\alpha_w=\frac{g^2}{4\pi}} T = 120T\left(\frac{g^2}{4\pi}\right)^5 \overset{\text{nucleation}}{\to} 120T_N\left(\frac{0.65^2}{4\pi}\right)^5 \approx 4.5\times 10^{-4}\ \text{GeV}. \quad \text{(A5)}$$

(h) The strong sphaleron rate [37]

$$\Gamma_{\rm ss} = 14\alpha_s^4 T \approx 0.26\ \text{GeV}. \quad \text{(A6)}$$

(i) Thermal width [38]:

$$\Gamma_{\rm leptons} \approx 2\times 10^{-3}T, \qquad \Gamma_{\rm quarks} \approx 0.16T. \quad \text{(A7)}$$

The temperature during nucleation is $T_N = 88$ GeV, and for the SM we use $\mathcal{R} = \frac{15}{4}$.

Thermal functions:

(a) The source is given by [14,39]

$$S_f(z;T) = \frac{v_w N_c^f}{\pi^2}\text{Im}(m_f' m_f^*) J_f(T) = \frac{v_w N_c^f {y_{\rm SM}^f}^2}{2\pi^2 v_0^2} J_f(T) h^3(z) h'(z) \times \kappa_I^f, \quad \text{(A8)}$$

$$J_f(T) = \int_0^\infty \frac{k^2 dk}{\omega_L^f \omega_R^f}\text{Im}\left[\frac{n_f(\mathcal{E}_L^f) - n_f(\mathcal{E}_R^{f*})}{(\mathcal{E}_L^f - \mathcal{E}_R^{f*})^2}(\mathcal{E}_L^f \mathcal{E}_R^{f*} - k^2) + \frac{n_f(\mathcal{E}_L^f) + n_f(\mathcal{E}_R^f)}{(\mathcal{E}_L^f + \mathcal{E}_R^f)^2}(\mathcal{E}_L^f \mathcal{E}_R^f + k^2)\right]. \quad \text{(A9)}$$

For the background Higgs boson field we use the kink solution:

$$h = \frac{v_N}{2}\left(1 + \tanh\left(\frac{z}{L_w}\right)\right). \quad \text{(A10)}$$

TABLE III. Relaxation rates (for the broken phase), and Yukawa rate (for both phases), calculated from [17].

Particle	Γ_M^B (GeV)	Γ_Y (GeV)
τ	4.9×10^{-3}	5.6×10^{-4}
μ	1.7×10^{-5}	2.0×10^{-6}
e	3.9×10^{-10}	4.4×10^{-11}
t	102	2.6
c	4.7×10^{-3}	1.6×10^{-4}
u	1.4×10^{-8}	4.7×10^{-10}
b	5.3×10^{-2}	1.7×10^{-3}
s	2.7×10^{-5}	9.0×10^{-7}
d	6.5×10^{-8}	2.1×10^{-9}

(b) The frequencies, energies and Fermi- Dirac distributions are

$$\omega_{L,R}^{f_i}(k) = \sqrt{k^2 + \text{Re}(\delta m^2_{f_{iL,R}}(T))}, \quad \mathcal{E}_L^{f_i} = \omega_{L,R}^{f_i}(k) - i\Gamma_{f_i}, \quad n_f(\mathcal{E}) = \frac{1}{e^{\frac{\mathcal{E}}{T}} + 1} \quad \text{(A11)}$$

(c) The thermal masses are given by [40]

$$\begin{aligned}
\text{Re}(\delta m^2_{L_{Li}}(T)) &= \left(\frac{3}{32}g^2 + \frac{1}{32}g'^2 + \frac{1}{16}y^2_{e_i}\right)T^2 \equiv a^2_{L_{Li}}T^2,\\
\text{Re}(\delta m^2_{e_{iR}}(T)) &= \left(\frac{1}{8}g'^2 + \frac{1}{8}y^2_{e_i}\right)T^2 \equiv a^2_{e_{Ri}}T^2,\\
\text{Re}(\delta m^2_{Q_{Li}}(T)) &= \left(\frac{1}{6}g_s^2 + \frac{3}{32}g^2 + \frac{1}{288}g'^2 + \frac{1}{16}y^2_{u_i} + \frac{1}{16}y^2_{d_i}\right)T^2 \equiv a^2_{Q_{Li}}T^2,\\
\text{Re}(\delta m^2_{u_{iR}}(T)) &= \left(\frac{1}{6}g_s^2 + \frac{1}{18}g'^2 + \frac{1}{8}y^2_{u_i}\right)T^2 \equiv a^2_{u_{Ri}}T^2,\\
\text{Re}(\delta m^2_{d_{iR}}(T)) &= \left(\frac{1}{6}g_s^2 + \frac{1}{72}g'^2 + \frac{1}{8}y^2_{d_i}\right)T^2 \equiv a^2_{d_{Ri}}T^2,\\
\text{Re}(\delta m^2_h(T)) &= \left(\frac{3}{16}g^2 + \frac{1}{16}g'^2 + \frac{1}{12}\sum_{i=e,\mu,\tau} y^2_{e_i} + \frac{1}{4}\sum_{i=u,c,t} y^2_{u_i} + \frac{1}{4}\sum_{i=d,s,b} y^2_{d_i}\right)T^2 \equiv a_h^2 T^2.
\end{aligned} \quad \text{(A12)}$$

(d) The finite temperature degrees of freedom are given by [10]

$$k_{f_i}(a_{f_i}) = k_0^{f_i}\frac{6}{\pi^2}\int_{a_{f_i}}^\infty dx \frac{xe^x}{(e^x \pm 1)^2}\sqrt{x^2 - a_{f_i}^2}. \quad \text{(A13)}$$

where k_0^f is the number of degrees of freedom, and $+$ $(-)$ is for fermions (the Higgs boson).

APPENDIX B: SOLVING THE SET OF TRANSPORT EQUATIONS: THE TWO-STEP APPROACH

In this Appendix we summarize the analytic techniques used to calculate the produced baryon asymmetry, similarly to Ref. [17]. We used the two-step approach: First we solve the set of transport equations, given in Eq. (10). Then, the BAU is obtained by summing over the left-handed number densities and considering the weak sphaleron process.

1. Reduction of dimensions

The left hand side of Eq. (10) can be written as a one-dimensional second-order differential equation with respect to the bubble wall dimension denoted z [18],

$$\partial f \equiv \partial_\mu f^\mu = \frac{\partial f^0}{\partial t} - \vec{\nabla}\cdot\vec{f} = \underbrace{\frac{\partial z}{\partial t}}_{\equiv v_w}\underbrace{\frac{\partial f^0}{\partial z}}_{f'} + \vec{\nabla}\cdot(-D_f\vec{\nabla}f^0)$$
$$= v_w f' - D_f\underbrace{\nabla^2 f^0}_{\equiv f''} = v_w f' - D_f f'', \tag{B1}$$

where we used Fick's first law and the diffusion approximation.

2. Reduction of order

We can solve this set of $N = 16$- second-order differential equations by reduction of order:

$$g_{f_i} \equiv f_i', \quad \vec{f} = (\vec{U}_R\ \ \vec{D}_R\ \ \vec{Q}_L\ \ \vec{E}_R\ \ \vec{L}_L\ \ h),\ \ \vec{\chi} = (\vec{f}\ \ \vec{g}_f)^T.$$
$$\vec{\chi}' = \begin{pmatrix} 0 & \mathbb{1}_{NxN} \\ \hat{\Gamma} & \hat{V} \end{pmatrix}\vec{\chi} + \vec{S} \equiv \hat{K}\vec{\chi} + \vec{S}. \tag{B2}$$

We are left with $2N$ first-order differential equations. Then, $\hat{K}$ can be diagonalized numerically, e.g., by using MATLAB.

3. Numerical diagonalization

The solution for the symmetric phase is given by

$$\vec{\chi}^S = \sum_{i=1}^{2N} C_i^S e^{\lambda_i^S z}\vec{u}_i^S \equiv \hat{\Phi}^S(z)\vec{C}^S,$$
$$\hat{\Phi}^X_{i,j}(z) = e^{\lambda^X_{jj}z}(\vec{u}^X_j)_i. \tag{B3}$$

where C_j's are constants, λ_j are the eigenvalues, and $\vec{u}_j$'s are the eigenvectors. We define

$$\hat{\lambda} = \mathrm{diag}(\lambda_i) \qquad i = [1:2N]. \tag{B4}$$

$$\hat{\phi} = \begin{pmatrix} | & | & & | \\ \vec{u}_1 & \vec{u}_2 & \dots & \vec{u}_{2N} \\ | & | & & | \end{pmatrix} \tag{B5}$$

Accordingly,

$$\hat{\Phi}_{i,j}(z) = \hat{\phi}_{ij}e^{\hat{\lambda}_{jj}z} = \begin{pmatrix} | & | & & | \\ e^{\lambda_1 z}\vec{u}_1 & e^{\lambda_2 z}\vec{u}_2 & \dots & e^{\lambda_{2N}z}\vec{u}_{2N} \\ | & | & & | \end{pmatrix} \tag{B6}$$

The full solution in the broken phase is obtained by variation of parameters to be

$$\vec{\chi}^B = \hat{\Phi}^B(z)\vec{C}^B + \hat{\Phi}^B(z)\int_0^z (\hat{\Phi}^B(x))^{-1}\vec{S}(x)\,dx. \tag{B7}$$

4. Boundary conditions

(a) The integration constants of the divergent modes in the symmetric phase (correspond to $\lambda_j^S \le 0$) are set to zero,

$$C^S_{0-} = 0. \tag{B8}$$

(b) The positive eigenvalues in the broken phase, C_j^{B+} (correspond to $\lambda_j^B > 0$), are chosen such that they cancel the divergent part of the full solution at infinity:

$$\vec{C}^B_+ = -\int_0^\infty (\hat{\Phi}^B_+(x))^{-1}\vec{S}(x)\,dx. \tag{B9}$$

(c) We demand continuity at $z = 0$.

(i) In the symmetric phase we have

$$\vec{\chi}^S_i(z\to 0^-) = \hat{\phi}^S_{ij}\vec{C}^S_j = \hat{\phi}^S_{i+}\vec{C}^S_+. \tag{B10}$$

(ii) In the broken phase we have

$$\vec{\chi}^B_i(z\to 0^+) = \hat{\phi}^B_{ij}\vec{C}^B_j = \hat{\phi}^B_{i(0-)}\vec{C}^B_{0-} + \underbrace{\hat{\phi}^B_{i+}\vec{C}^B_+}_{\equiv b_i}$$
$$= \hat{\phi}^B_{i(0-)}\vec{C}^B_{0-} + b_i. \tag{B11}$$

Continuity is then

$$\hat{\phi}^S_{i+}\vec{C}^S_+ \stackrel{!}{=} \hat{\phi}^B_{i(0-)}\vec{C}^B_{0-} + b_i \to \hat{\phi}^S_{i+}\vec{C}^S_+ - \hat{\phi}^B_{i(0-)}\vec{C}^B_{0-} = b_i. \tag{B12}$$

We obtain a linear set of equations,

$$\hat{\phi}_{SB} \equiv \left(\begin{array}{c|c} | & | \\ \hat{\phi}^S_{i+} & \hat{\phi}^B_{i(0-)} \\ | & | \end{array}\right), \qquad \vec{C}_{SB} \equiv \begin{pmatrix} \vec{C}^S_+ \\ -\vec{C}^B_{0-} \end{pmatrix},$$
$$\hat{\phi}_{SB}\vec{C}_{SB} \stackrel{!}{=} b_i. \tag{B13}$$

Solving it sets the rest of the coefficients.

5. The solution

The BAU is then given by

$$Y_B = \frac{3\Gamma_{\mathrm{ws}}}{2D_q\alpha_+ s}\int_0^{-\infty} e^{-\alpha_- x}n_L(x)\,dx, \tag{B14}$$

where n_L is the density of left handed particles in the symmetric phase (where the weak sphaleron process is efficient),

$$n_L(z) = \sum_{i=1}^{3} (Q_{Li}(z) + L_{Li}(z)), \tag{B15}$$

and

$$\alpha_\pm = \frac{1}{2D_q}\left(v_w \pm \sqrt{4D_q\Gamma_{\rm ws}\mathcal{R} + v_w^2}\right). \tag{B16}$$

[1] M. Tanabashi *et al.* (Particle Data Group), Phys. Rev. D **98**, 030001 (2018).
[2] P. A. R. Ade *et al.* (Planck Collaboration), Astron. Astrophys. **594**, A13 (2016).
[3] J. M. Cline, arXiv:hep-ph/0609145.
[4] D. E. Morrissey and M. J. Ramsey-Musolf, New J. Phys. **14**, 125003 (2012).
[5] A. D. Sakharov, Pis'ma Zh. Eksp. Teor. Fiz. **5**, 32 (1967) [JETP Lett. **5**, 24 (1967)]; Usp. Fiz. Nauk **161**, 61 (1991), https://ufn.ru/en/articles/1991/5/h/ [Sov. Phys. Usp. **34**, 392 (1991)].
[6] M. B. Gavela, P. Hernandez, J. Orloff, and O. Pene, Mod. Phys. Lett. A **09**, 795 (1994).
[7] P. Huet and E. Sather, Phys. Rev. D **51**, 379 (1995).
[8] A. M. Sirunyan *et al.* (CMS Collaboration), Eur. Phys. J. C **80**, 3 (2020).
[9] G. Aad *et al.* (ATLAS Collaboration), J. High Energy Phys. 03 (2020) 145.
[10] J. de Vries, M. Postma, J. van de Vis, and G. White, J. High Energy Phys. 01 (2018) 089.
[11] J. de Vries, M. Postma, and J. van de Vis, J. High Energy Phys. 04 (2019) 024.
[12] E. Fuchs, M. Losada, Y. Nir, and Y. Viernik, J. High Energy Phys. 05 (2020) 056.
[13] E. Fuchs, M. Losada, Y. Nir, and Y. Viernik, Phys. Rev. Lett. **124**, 181801 (2020).
[14] C. Lee, V. Cirigliano, and M. J. Ramsey-Musolf, Phys. Rev. D **71**, 075010 (2005).
[15] V. A. Kuzmin, V. A. Rubakov, and M. E. Shaposhnikov, Phys. Lett. **155B**, 36 (1985).
[16] M. Joyce, T. Prokopec, and N. Turok, Phys. Rev. D **53**, 2930 (1996).
[17] E. Fuchs, M. Losada, Y. Nir, and Y. Viernik, J. High Energy Phys. 07 (2021) 060.
[18] A. G. Cohen, D. B. Kaplan, and A. E. Nelson, Phys. Lett. B **336**, 41 (1994).
[19] H. K. Guo, Y. Y. Li, T. Liu, M. Ramsey-Musolf, and J. Shu, Phys. Rev. D **96**, 115034 (2017).
[20] G. F. Giudice and M. E. Shaposhnikov, Phys. Lett. B **326**, 118 (1994).
[21] D. J. H. Chung, B. Garbrecht, M. J. Ramsey-Musolf, and S. Tulin, Phys. Rev. D **81**, 063506 (2010).
[22] D. de Florian *et al.* (LHC Higgs Cross Section Working Group), Deciphering the nature of the Higgs sector, in *Handbook of LHC Higgs Cross Sections*, edited by D. de Florian, C. Grojean, F. Maltoni, C. Mariotti, A. Nikitenko, M. Pieri, P. Savard, M. Schumacher, and R. Tanaka (CERN, 2017), Vol. 2, 10.23731/CYRM-2017-002.
[23] A. M. Sirunyan *et al.* (CMS Collaboration), Phys. Rev. Lett. **121**, 121801 (2018).
[24] G. Aad *et al.* (ATLAS Collaboration), Phys. Lett. B **812**, 135980 (2021).
[25] R. Carlin (CMS Collaboration), CMS highlights, in *40th International Conference on High Energy Physics (ICHEP2020)* (Sissa Medialab, Prague, 2020), https://indico.cern.ch/event/868940/contributions/3905676/attachments/2084164/3501074/CMShighlights_ICHEP2020_V4.pdf.
[26] S. Dittmaier *et al.* (LHC Higgs Cross Section Working Group), Handbook of LHC Higgs Cross Sections: 1. Inclusive Observables, Technical Report No. CERN-2011-002; CERN-2011-002, Geneva 2011, 10.5170/CERN-2011-002.
[27] G. Aad *et al.* (ATLAS Collaboration), Phys. Lett. B **801**, 135148 (2020).
[28] V. Andreev *et al.* (ACME Collaboration), Nature (London) **562**, 355 (2018).
[29] C. Abel *et al.* (nEDM Collaboration), Phys. Rev. Lett. **124**, 081803 (2020).
[30] J. Brod and E. Stamou, J. High Energy Phys. 07 (2021) 080.
[31] Y. T. Chien, V. Cirigliano, W. Dekens, J. de Vries, and E. Mereghetti, J. High Energy Phys. 02 (2016) 011.
[32] G. Panico, A. Pomarol, and M. Riembau, J. High Energy Phys. 04 (2019) 090.
[33] J. Brod, U. Haisch, and J. Zupan, J. High Energy Phys. 11 (2013) 180.
[34] W. Altmannshofer, J. Brod, and M. Schmaltz, J. High Energy Phys. 05 (2015) 125.
[35] J. Brod and D. Skodras, J. High Energy Phys. 01 (2019) 233.
[36] D. Bodeker, G. D. Moore, and K. Rummukainen, Phys. Rev. D **61**, 056003 (2000).
[37] G. D. Moore and M. Tassler, J. High Energy Phys. 02 (2011) 105.
[38] P. Elmfors, K. Enqvist, A. Riotto, and I. Vilja, Phys. Lett. B **452**, 279 (1999).
[39] V. Cirigliano, M. J. Ramsey-Musolf, S. Tulin, and C. Lee, Phys. Rev. D **73**, 115009 (2006).
[40] K. Enqvist, A. Riotto, and I. Vilja, Phys. Lett. B **438**, 273 (1998).